33rd Annual International Conference of the IEEE EMBS
Boston, Massachusetts USA, August 30 - September 3, 2011

Microaneurysm Detection with Radon Transform-based Classification on Retina Images

L. Giancardo, *Student Member, IEEE*, F. Meriaudeau, *Member, IEEE*, T. P. Karnowski, *Member, IEEE*, Y. Li, *Member, IEEE*, K. W. Tobin Jr, *Senior Member, IEEE* and E. Chaum, *Member, IEEE*

***Abstract*—The creation of an automatic diabetic retinopathy screening system using retina cameras is currently receiving considerable interest in the medical imaging community. The detection of microaneurysms is a key element in this effort. In this work, we propose a new microaneurysms segmentation technique based on a novel application of the radon transform, which is able to identify these lesions without any previous knowledge of the retina morphological features and with minimal image pre-processing. The algorithm has been evaluated on the Retinopathy Online Challenge public dataset, and its performance compares with the best current techniques. The performance is particularly good at low false positive ratios, which makes it an ideal candidate for diabetic retinopathy screening systems.**

I. INTRODUCTION

Diabetic retinopathy (DR) is the leading cause of new cases of blindness among adults aged between 20 and 74 years. The Centers for Disease Control and Prevention estimates that 25.8 million people currently have diabetes mellitus in the United States alone. The World Diabetes Foundation estimates that over 439 million people will have diabetes worldwide by 2030. New high-quality mydriatic and non-mydriatic fundus cameras have the potential to greatly improve our ability to effectively screen the retinas of a large population and to identify patients with vision threatening disease complications. In fact, it is estimated that timely treatment with laser therapy can reduce the development of severe vision loss by 50% to 60% in a patient with DR [1].

Microaneurysms (MAs) are a common and often early manifestation of DR. They are dilated, aneurismal retina vessels that appear as small red dots in colour retina fundus images. These lesions can leak fluid and blood into the retina, leading to vision threatening exudates, macular edema and hemorrhages. These MAs are the primary target lesions for laser treatment of macular edema. As such, the MA detector is an attractive candidate for an automatic screening system able to detect early findings of DR.

These studies were supported in part by grants from Oak Ridge National Laboratory, the National Eye Institute, (EY017065), by an unrestricted UTHSC Departmental grant from Research to Prevent Blindness (RPB), New York, NY, by The Plough Foundation, Memphis, TN and by the Regional Burgundy Council, France.

L. Giancardo is with the University of Burgundy and the Oak Ridge National Laboratory (e-mail: giancardol@ornl.gov).

F. Meriaudeau is with the University of Burgundy, Le Creusot, 71200 France.

T.P. Karnowski and K.W. Tobin, Jr are with the Oak Ridge National Laboratory, Oak Ridge, TN 37831 USA.

E. Chaum is an RPB Senior Scientist. E. Chaum and Y. Li are with the University of Tennessee Health Science Center, Memphis TN 38163 USA.

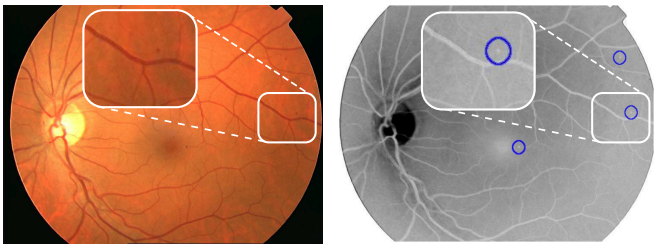

(a) (b)

Fig. 1. (a) Example of a retina fundus image with a MA magnified; (b) Inverted green channel of (a) with MAs automatically detected.

In the early literature [2, 3, 4], algorithms were developed to detect MAs (and other small round hemorrhages) in fluorescein angiograms. They employed a series of morphological operations which remove the vasculature, leaving the other small structures representing the MAs. These approaches perform well on fluorescein angiograms but are not satisfactory on colour fundus images. Fluorescein angiograms use an intravenous contrast agent, therefore the contrast between vessels/lesions and background is much greater than that of colour fundus images making the development of the algorithm straightforward. Unfortunately, the injection of the contrast agent is not a risk-free process and requires more highly trained personnel to deliver than a simple fundus photograph, hence it is not an optimal approach for broad-based DR screening.

In 2008, Niemeijer et al. [5] announced the Retinal Online Challenge (ROC). The aim was to focus the efforts of the research community towards the creation of algorithms for the detection of MAs on colour fundus images, by evaluating their performance on a common dataset. Two sets of 50 images captured by different cameras that imaged the same area of the retina (45 degrees) were released to the research community together with a common evaluation modality. This allowed a fair comparison between algorithms developed by different groups. So far, 11 groups have participated in the challenge. The two top performing techniques [6, 7] are based on a combination of multiple techniques that require various intermediate steps such as vessel segmentation and multiple classifiers.

In a previous paper [8], we have shown how the Radon Transform is particularly suited for the compact representation of Gaussian-like structure such as MAs. In this work, we analyse the radon space with a new set of features classified through Principal Component Analysis (PCA) and a Support Vector Machine (SVM) which increase the performance sub-

stantially. This method is streamlined, does not require a vessel segmentation and is easily trainable.

In Section II we present the details of the algorithm developed; Section III discusses the characteristics of the ROC dataseta and our samples selection approach; Section IV presents the results; finally, Section V concludes with a discussion of the method and results.

II. METHOD

Our method starts with a very conservative candidates selection phase, in which we rule out the obvious areas that cannot contain any type of dark lesion. This phase is required only to avoid unnecessary computations. Then, we split the image into small windows and we proceed with the creation of the Radon based features. In the final phase, we assign a score representing the likelihood of containing a MA to each window in the image.

A. Feasibility Study Data

The algorithm was developed on 5 images selected from different datasets. One of these images came from the ROC training set. A total of 122 window samples were manually selected with the following distribution: 60 windows containing MAs, 38 windows containing vessels and 24 windows containing only background.

B. Candidates Selection

The green channel I_g is extracted from the original RGB image and resized (with bilinear interpolation) such that the original ratio height/width remain unmodified and the new width is 768 pixels. The black background around the field of view (FOV) is detected with a simple region growing method [9] and stored in I_{mask}. I_g is cropped based on the redundant rows and column of I_{mask} in order to maximize the FOV. Then, the background is estimated by the means of a large median filter on I_{gi}, the inverted version of I_g (see Fig. 1.b). The dimension of the median filter is 4% the size of I_{gi}. The background image is subtracted from I_{gi} obtaining an image whose distribution is naively assumed to be Gaussian and normalized with $\mu = 0.5$ and $\sigma = 0.2$. All the pixels not laying between 0 and 1 are considered "outliers" and changed to the nearest valid value. While the value of μ was chosen to be in the middle of the allowed range, the value of σ was empirically derived from the 5 images employed in the feasibility study, so that a high percentage of the image pixels ($\sim$95%) would stay in the allowed range. I_{norm} is the image generated by this type of normalization, which allows to compare the pixel values across images with different pigmentation, illumination and contrast. On the top row of Fig. 2, details of I_{gi} (I^i_{win}) are shown together with the normalized version (I^i_{winEq}).

The pixels selected as candidates are those having a value greater than a hard threshold $th = 0.58$ and that do not lie on I_{mask}. th is selected to be a very conservative value such that all the areas corresponding to the MAs of the 5 images in the feasibility study are included.

C. Radon Transform Analysis

The Radon based features are calculated on I_{gi}. This image did not undergo any type of preprocessing apart from cropping, resizing and pixel value inversion operations. By employing I_{gi} directly, we avoid the small artefacts that are inherent to the background subtraction operation, especially on images with a substantial JPG compression such as the ones found in the ROC dataset.

The image is partitioned in 5×5 pixel windows in order to form a grid-like pattern. Each window is deemed as valid if it contains at least one candidate pixel. Each valid window is centered on the pixel with the highest value in its local neighbourhood, in order to have the suspected MA in the middle of the window. The Radon transform is calculated on a 17×17 neighbourhood (I^i_{win}), with scanning angles between 0° and 165° spaced of an interval of 15°. Because of the non-isometric support (the window is a square), at some angles the Radon projections will go through an unequal number of pixels, which leads to an image containing coefficients biased towards certain locations. This "Radon transform bias" problem is overcome by normalizing each projection ray by the number of pixels that it crosses as described in [8]. Fig. 2 shows some examples of the Radon space obtained (R^i).

We attempt to capture the characteristics of the radon space that separate the MAs from other dark structures, such as vessels or pigmentation noise, with a straightforward analysis.

$$R^i_\mu(x) = \frac{1}{\phi}\sum_{n=1}^{\phi} R^i(n,x) \quad 0 \le x < \rho \tag{1}$$

$$R^i_\sigma(x) = \sqrt{\frac{1}{\phi-1}\sum_{n=1}^{\phi}[R^i(n,x) - R_\mu(x)]^2} \quad 0 \le x < \rho \tag{2}$$

where i is the index of a window, R^i is the window in the normalized Radon space having on the horizontal axis the different angles of projections and on the vertical one the number of projections for each angle. ϕ is the number of projection angles and ρ is the number of projection rays.

Note that R^i_μ is a vector containing the mean across the rows of R^i. In the case of a MA, it will have a strong maximum in the middle, even if another prominent structure (such as a vessel) is at the periphery of the window I^i_{win}. Since we want to use R^i_μ as features for classification purposes, we need to make these measurements as homogeneous as possible. The fact that the radon transform is calculated on a non-normalized image might create problems in this regard. Therefore we employ the first derivative $\frac{d}{dx}R^i_\mu(x)$, which is able to capture the location of maxima and minima without using absolute values (that differ depending on the background pigment, contrast and illumination).

In some instances, there is a strong resemblance between MAs and vessel bifurcations. By employing R^i_σ (i.e. the standard deviation across the rows of R^i) we can determine if the central crest of R^i is constant or not. In the first case, R^i is very likely to contain a MA, but in the second case some type of vessel bifurcation. We add R^i_σ to the feature vector unchanged because the standard deviation is inherently

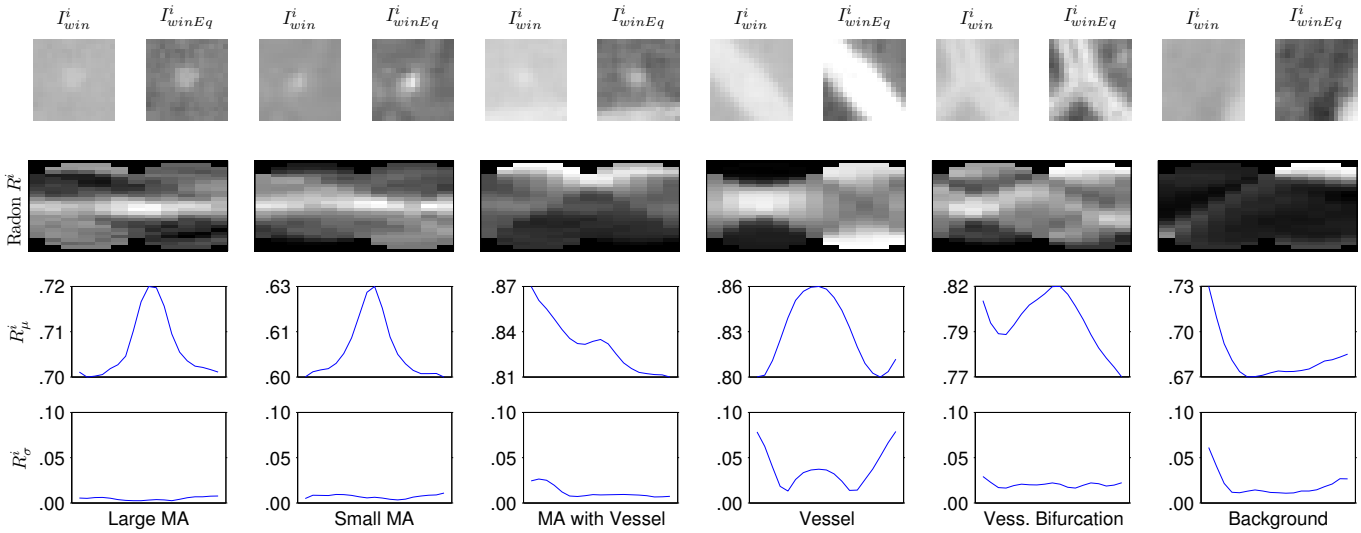

Fig. 2. Visualization of Radon transform analysis. Each column represents the analysis for a single window. In the top row, the original (I^i_{win}) and the equalized (I^i_{winEq}) windows are shown; in the second row, the normalized radon space (R^i) is shown; in the third row, the vectors R^i_μ are displayed (at different scales); in the last row, the vectors R^i_σ are shown.

independent of different types of backgrounds. Fig. 2 shows the various analysis steps for different sample classes.

Finally, the feature vector is generated as $F^i = \left(\frac{\frac{d}{dx}R^i_\mu}{R^i_\sigma}\right)$ and by removing all the dimensions always having a value of 0.

D. Classification

The original feature vector F^i has 37 dimensions (this number may vary depending on the implementation of the Radon transform). The samples are normalized so that the samples distribution has 0 mean and a standard deviation of 1 across each dimensions. Then, all F^i are projected to an hyperplane of 10 dimensions obtaining F^i_{pca} through Principal Component Analysis (PCA). During the feasibility study, we have estimated that this dimensionality reduction maintains 95% of the original variance, hence little information is lost during the process and making possible the reduction of the data dimensionality. At the feasibility study stage, this was confirmed by a 10-fold classification test: the SVM classifier obtained a score of 0.89 of the Area Under the ROC Curve (AUC) on the original F^i and a score of 0.96 AUC after PCA dimensionality reduction.

As already mentioned, the F^i_{pca} is classified with a SVM. We employed a 3 degrees radial basis kernel with $\varepsilon = 0.001$ and the estimation of the probability with the method implemented in the LIBSVM library by J.C. Platt [10].

The calculation of the probability of being a MA is a combination of the SVM probability output and the average grey level at the centre of the equalized window of I^i_{winEq} 3×3 neighbourhood. The two probabilities are combined by a multiplication as suggested by the unnormalized Bayes rule.

The final step is a non maxima suppression in the matrix containing the MA probabilities, so that neighbouring MAs are not considered separate detections but a single one. This is performed with a morphological closing operation with 12×12 structuring element, followed by a blob analysis. Fig. 1 shows an example of the MA detection.

III. MATERIALS AND TRAINING STRATEGY

We evaluated the MA detection algorithm on the ROC dataset. In the this dataset, four retinal experts annotated all the small red lesions (MA and round hemorrhages) by labelling them as MA or irrelevant lesions. The set was divided in two: training and testing (composed of 50 images each). For the former, the global judgement of the experts was publicly released via an XML file, which did not contain the source of the decision but only the global labels combined together with an OR operation. This maximized the global sensitivity at a price of a certain number of false positives. The lesion labels on the test set were withheld in order to avoid training on the testing set. In this case, the gold standard of the experts' judgement was created with a voting system for a better trade off between sensitivity and false positives.

A novel training strategy was adopted for the classifier. First, we hand selected all the unambiguous MAs from the ROC training set and used them as positive examples. Then, we manually selected a handful of negative examples and trained a "baseline" classifier. At this point, we employed an on-line training technique to update the classifier with negative examples. This is possible through a GUI (that we developed) that is able to add a negative sample, train the classifiers and show the detection in real time. We picked an image showing a few MAs (from the training set), and we added negative samples up until we were satisfied with the detection. This approach allows us to add only the negative examples that are effectively useful to the MAs classification leaving the uncertain structures out of the training set. By minimizing the samples required, we avoid overtraining and greatly simply the whole training process. We trained the classifier used for these tests in around 20 minutes.

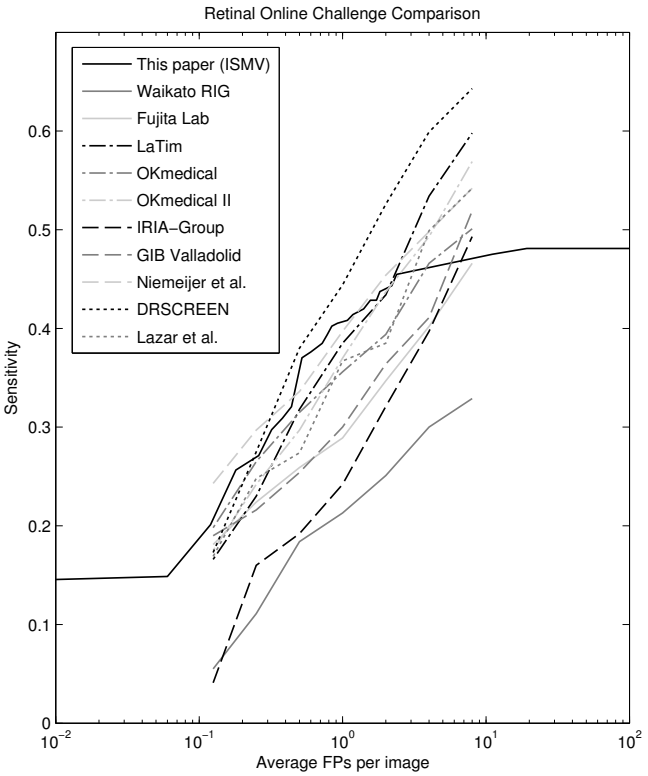

Fig. 3. Comparison of the FROC curves of all the groups that participated at the ROC. On the y-axis, the average image based sensitivity is displayed, on the x-axis, the average number of false positives (FPs) found on each image is shown. Note that the FPs are plotted on a logarithmic scale.

IV. RESULTS

Fig. 3 shows the results of the comparative FROC analysis on the Retinopathy Online Challenge data. Our technique compared very well with other submissions, particularly at a low false positive (FP) rate. This can be better appreciated in Table I. Relatively high performance at a low FPs rate are particularly interesting for a screening setting, where it is not important to find all the MAs, but to find enough of them to decide that the patient needs referral.

TABLE I
RETINOPATHY ONLINE CHALLENGE COMPARISON

Group	Global Score	Sensitivity at 0.5 FPs
This paper (ISMV)	0.375	0.366
Waikato RIG	0.206	0.184
Fujita Lab	0.310	0.259
LaTIM	0.381	0.318
OKmedical	0.357	0.315
OKmedical II	0.369	0.297
IRIA-Group	0.264	0.192
GIB Valladolid	0.322	0.254
Niemeijer et al. [7]	0.395	0.336
DRSCREEN [6]	*0.434*	*0.380*
Lazar et al.	0.355	0.274

with the exception of our results, the table shows results in the order found on the ROC website http://roc.healthcare.uiowa.edu/ as of March 2011.

In the current unoptimized Matlab implementation, the whole analysis process takes ∼12 seconds per image on a 1.6 GHz machine with 4 GB of RAM. This figure can be easily reduced because more than half of the total time is spent on the FOV detection, preprocessing and window alignment. Also, the algorithm has the potential of greatly benefit of parallelization because of independent nature of the window based analysis.

V. CONCLUSIONS AND DISCUSSION

In this paper we present a MA detector based on a novel radon-based approach. The radon based features allows the detection of MAs directly on the original image without vessel or optic nerve segmentation. Also, they are inherently able to identify MAs of different sizes without multiscale analysis. Another advantage of the algorithm, is the ease of training. It does not require a large dataset, once some examples of MAs are shown to the classifier, it is simply a matter of dynamically selecting the negative examples on one or two images to make the algorithm "converge" to the desired performance.

This algorithm seems particularly well suited as a component of DR screening applications. In the near future, we will test the algorithm performance in this context and we will couple it with other techniques to determine if combining approaches improve its sensitivity to subtle MAs.

REFERENCES

[1] Centers for Disease Control and Prevention, "National diabetes fact sheet: national estimates and general information on diabetes and prediabetes in the united states," U.S. Department of Health and Human Services, Centers for Disease Control and Prevention, Tech. Rep., 2011.

[2] C. E. Baudoin, B. J. Lay, and J. C. Klein, "Automatic detection of microaneurysms in diabetic fluorescein angiography." *Rev Epidemiol Sante Publique*, vol. 32, no. 3-4, pp. 254–261, 1984.

[3] T. Spencer, J. A. Olson, K. C. McHardy, P. F. Sharp, and J. V. Forrester, "An image-processing strategy for the segmentation and quantification of microaneurysms in fluorescein angiograms of the ocular fundus." *Comput Biomed Res*, vol. 29, no. 4, pp. 284–302, Aug 1996.

[4] J. A. Frame, P. E. Undrill, M. J. Cree, J. A. Olson, K. C. McHardy, P. F. Sharp, and J. V. Forrester, "A comparison of computer based classification methods applied to the detection of microaneurysms in ophthalmic fluorescein angiograms," *Computers in Biology and Medicine*, vol. 28, pp. 225–238, 1998.

[5] M. Niemeijer, B. van Ginneken, M. J. Cree, A. Mizutani, G. Quellec, C. I. Sanchez, B. Zhang, R. Hornero, M. Lamard, C. Muramatsu, X. Wu, G. Cazuguel, J. You, A. Mayo, Q. Li, Y. Hatanaka, B. Cochener, C. Roux, F. Karray, M. Garcia, H. Fujita, and M. D. Abramoff, "Retinopathy online challenge: Automatic detection of microaneurysms in digital color fundus photographs," *IEEE Transactions on Medical Imaging*, vol. 29, no. 1, pp. 185–195, Jan. 2010.

[6] B. Antal, I. Lazar, and A. Hajdu, "An ensemble-based system for microaneurysm detection," University of Debrecen, Hungary, Tech. Rep., 2010. [Online]. Available: http://roc.healthcare.uiowa.edu/results/documentation/drscreen.pdf

[7] M. Niemeijer, B. van Ginneken, J. Staal, M. S. A. Suttorp-Schulten, and M. D. Abramoff, "Automatic detection of red lesions in digital color fundus photographs," *IEEE Transactions on Medical Imaging*, vol. 24, no. 5, pp. 584–592, 2005.

[8] L. Giancardo, F. Meriaudeau, T. Karnowski, K. Tobin Jr, Y. Li, and E. Chaum, "Microaneurysms detection with the radon cliff operator in retinal fundus images," in *Proceedings of SPIE*, vol. 7623, 2010, p. 76230U.

[9] L. Giancardo, F. Meriaudeau, T. P. Karnowski, E. Chaum, and K. Tobin, *Quality Assessment of Retinal Fundus Images using ELVD*. IN-TECH, 2010, ch. New Developments in Biomedical Engineering, pp. 201–224.

[10] C.-C. Chang and C.-J. Lin, *LIBSVM: a library for support vector machines*, 2001. [Online]. Available: http://www.csie.ntu.edu.tw/~cjlin/libsvm